

The synthesis and characterization of 1 1 1 1 type diluted ferromagnetic semiconductor
(La_{1-x}Ca_x)(Zn_{1-x}Mn_x)AsO

This content has been downloaded from IOPscience. Please scroll down to see the full text.

2016 J. Phys.: Condens. Matter 28 026003

(<http://iopscience.iop.org/0953-8984/28/2/026003>)

View [the table of contents for this issue](#), or go to the [journal homepage](#) for more

Download details:

IP Address: 129.6.122.118

This content was downloaded on 10/02/2016 at 16:26

Please note that [terms and conditions apply](#).

The synthesis and characterization of 1 1 1 1 type diluted ferromagnetic semiconductor $(\text{La}_{1-x}\text{Ca}_x)(\text{Zn}_{1-x}\text{Mn}_x)\text{AsO}$

Cui Ding^{1,2}, Shengli Guo^{1,2}, Yao Zhao^{1,2}, Huiyuan Man^{1,2}, Licheng Fu^{1,2}, Yilun Gu^{1,2}, Zhouyang Wang^{1,2}, L Liu³, B A Frandsen³, S Cheung³, Y J Uemura³, T Goko^{3,4}, H Luetkens⁴, E Morenzoni⁴, Yang Zhao^{5,6} and F L Ning^{1,2}

¹ Department of Physics, Zhejiang University, Hangzhou 310027, People's Republic of China

² Collaborative Innovation Center of Advanced Microstructures, Nanjing 210093, People's Republic of China

³ Department of Physics, Columbia University, New York, NY 10027, USA

⁴ Laboratory for Muon Spin Spectroscopy, Paul Scherrer Institute, CH-5232 Villigen PSI, Switzerland

⁵ NIST center for Neutron Research, National Institute of Standards and Technology, Gaithersburg, MD 20899, USA

⁶ Department of Materials Science and Engineering, University of Maryland, College Park, MD 20742, USA

E-mail: ningfl@zju.edu.cn

Received 28 July 2015, revised 7 November 2015

Accepted for publication 23 November 2015

Published 17 December 2015



Abstract

We report the synthesis and characterization of a bulk form diluted magnetic semiconductor, $(\text{La}_{1-x}\text{Ca}_x)(\text{Zn}_{1-y}\text{Mn}_y)\text{AsO}$, with a layered crystal structure isostructural to that of the 1 1 1 1 type Fe-based high-temperature superconductor LaFeAsO and the antiferromagnetic LaMnAsO . With Ca and Mn codoping into LaZnAsO , the ferromagnetic ordering occurs below the Curie temperature $T_C \sim 30$ K. Taking advantage of the decoupled charge and spin doping, we investigate the influence of carrier concentration on the ferromagnetic ordering state. For a fixed Mn concentration of 10%, T_C increases from 24 K to 30 K when the Ca concentration increases from 5% to 10%. Further increase of Ca concentration reduces both the coercive field and saturation moment. Muon spin relaxation measurements confirm the ferromagnetically ordered state, and clearly demonstrate that $(\text{La}_{1-x}\text{Ca}_x)(\text{Zn}_{1-y}\text{Mn}_y)\text{AsO}$ shares a common mechanism for the ferromagnetic exchange interaction with $(\text{Ga,Mn})\text{As}$. Neutron scattering measurements show no structural transition in $(\text{La}_{0.90}\text{Ca}_{0.10})(\text{Zn}_{0.90}\text{Mn}_{0.10})\text{AsO}$ below 300 K.

Keywords: DMS, ferromagnetic order, muSR, carrier doping

(Some figures may appear in colour only in the online journal)

1. Introduction

The substitution of Mn for Ga and In in III–V semiconductors GaAs and InAs generates ferromagnetic ordering [1–8], which has attracted significant study of dilute magnetic semiconductors (DMS). When doping Mn up to $\sim 12\%$ in GaAs, the ferromagnetic Curie temperature T_C reaches ~ 200 K [9–11]. It is believed that T_C can reach as high as room temperature if more

Mn atoms are doped into the material [12]. The low chemical solubility of Mn^{2+} for Ga^{3+} , however, prevents a higher doping level of Mn. Additionally, the carriers and spins in $(\text{Ga,Mn})\text{As}$ compounds are induced simultaneously by Mn atoms, which makes it difficult to investigate the individual influence of charge and spin degrees of freedom on the ferromagnetism.

Recently, a series of bulk DMS systems derived from Fe-based superconductors [13–16] have been reported

[17–27], which have the advantage of decoupling spin- and carrier-doping. The first reported material is Li(Zn,Mn)As with $T_C \sim 50$ K [17]. In this system, spins are introduced by Mn atoms and carriers are introduced by excess Li atoms. The substitution of Mn for Zn instead of Ga solved the problem of low solubility of magnetic atoms in III–V DMSs. The fabrications of these new DMSs opened up a window to investigate the individual influence of carriers and local moments on the ferromagnetic ordering. The maximum T_C of these new DMSs has reached up to ~ 230 K in (Ba,K)(Zn,Mn) $_2$ As $_2$ with 15% Mn doping and 30% K doping [23].

The availability of bulk form specimens is another important feature. It realizes the possibility of investigation by nuclear magnetic resonance (NMR), muon spin relaxation (μ SR) and neutron scattering on DMSs. An NMR investigation of Li(Zn,Mn)P by Ding *et al* shows that Li(0) (zero means that there are no Mn atoms at the nearest neighbor(NN) Zn sites of Li) sites are under the influence of ferromagnetic Mn spin fluctuations [28], indicating that the carriers in Li(Zn,Mn)P indeed mediate the ferromagnetic exchange interaction. Comparing the μ SR results of 1 1 1 (Li(Zn,Mn)P), Li(Zn,Mn)As [17, 29], 1 1 1 ((La,Ba)(Zn,Mn)AsO) [19], 122 (Ba,K)(Zn,Mn) $_2$ As $_2$ [23] type bulk DMSs with that of (Ga,Mn)As [30], we find a universal linear trend between the static internal field parameter a_s and the ferromagnetic Curie temperature T_C [17, 19, 23, 29]. The linear relation indicates that they all share a common ferromagnetic mechanism.

In this paper, we report the successful synthesis of a new 1 1 1 type bulk DMS (La,Ca)(Zn,Mn)AsO, which is isostructural to the parent compound of Fe-based high-temperature superconductor LaFeAsO [14]. In this system, Ca $^{2+}$ substitution for La $^{3+}$ and Mn $^{2+}$ substitution for Zn $^{2+}$ introduce carriers and spins, separately. The main results are classified in two subgroups. The first group has the same doping level for Ca and Mn at 5%, 10% and 20%. For the second group, we fix the Mn concentration at 10% and increase the Ca doping level from 5% up to 30%. As mentioned in PRB Rapid Communication about (La,Ba)(Zn,Mn)AsO by Ding *et al*, Mn $^{2+}$ substitution for Zn $^{2+}$ in LaZnAsO alone does not induce ferromagnetic ordering [19]. Here, we substitute Ca for La inducing carriers and observe the static ferromagnetic order below $T_C \sim 30$ K for (La $_{0.90}$ Ca $_{0.10}$)(Zn $_{0.90}$ Mn $_{0.10}$)AsO. The resistivity of (La $_{1-x}$ Ca $_x$)(Zn $_{1-y}$ Mn $_y$)AsO shows a typical semiconducting behavior and the coercive field reaches ~ 1 T in (La $_{0.90}$ Ca $_{0.10}$)(Zn $_{0.90}$ Mn $_{0.10}$)AsO. Exploiting the decoupling of carrier- and spin-doping, we increase the Ca concentration while leaving the Mn doping fixed. The temperature dependent resistivity remains semiconducting even with Ca doping concentration up to 30%. We find that it is the best for ferromagnetic ordering to form when doping the same concentration of Ca and Mn. The ferromagnetic Curie temperature T_C , static spin freezing temperature T_f , saturation moment and coercive field all have a minimum value at 5% Ca doping and reach a maximum in (La $_{0.90}$ Ca $_{0.10}$)(Zn $_{0.90}$ Mn $_{0.10}$)AsO. The saturation moment and coercive field are reduced when the concentration of Ca is further increased. We performed μ SR and neutron scattering measurements for this system. The μ SR measurements demonstrate that (La $_{0.90}$ Ca $_{0.10}$)(Zn $_{0.90}$ Mn $_{0.10}$)AsO has a

common ferromagnetic mechanism with (Ga,Mn)As, (Ba,K)(Zn,Mn)AsO, Li(Zn,Mn)Pn (Pn = As, P) and (La,Ba)(Zn,Mn)AsO. In the whole temperature range of neutron scattering measurements, a structural phase transition is not observed.

2. Experiments

Polycrystalline specimens of (La $_{1-x}$ Ca $_x$)(Zn $_{1-y}$ Mn $_y$)AsO were synthesized through the solid-state reaction method at Zhejiang University. High-purity elements of La, Zn and As were mixed and heated at 900 °C in an evacuated silica tube for 10h to produce intermediate products LaAs and ZnAs. They were then mixed with ZnO, MnO and CaO with nominal concentrations and made into pellets. The mixture was then heated up to 1150 °C slowly and held for 40h before cooling down by shutting off the furnace. The polycrystals were characterized by x-ray powder diffraction (a PANalytical x-ray diffractometer with monochromatic Cu K $_{\alpha 1}$ radiation) at room temperature and dc magnetization by a quantum design superconducting quantum interference device (SQUID). The electrical resistance was measured on sintered pellets with the typical four-probe method. Zero-field (ZF) and longitudinal-field (LF) μ SR measurements were performed at the Paul Scherrer Institute and TRIUMF. Neutron scattering measurements were performed at the NIST Center for Neutron Research (NCNR) using the BT-1 powder Diffractometer.

3. Results and discussion

First, we examine the compound with the same Ca and Mn doping levels, including the parent compound. We show the powder x-ray diffraction patterns of (La $_{1-x}$ Ca $_x$)(Zn $_{1-x}$ Mn $_x$)AsO ($x = 0.00, 0.05, 0.10, 0.20$) in figure 1(a). Bragg peaks of the parent compound LaZnAsO can be well indexed by a tetragonal crystal structure of space group $P4/nmm$, as demonstrated by Reitveld refinement for LaZnAsO compound [19], with $a = 4.1027$ Å and $c = 9.0781$ Å. The crystal structure of LaZnAsO, a ZrCuSiAs-type tetragonal crystal structure is shown in figure 1(c), which is isostructural to the 1 1 1 type Fe-based high-temperature superconductors LaFeAsO [14] and antiferromagnetic LaMnAsO [31]. Lattice parameters for these four specimens are shown in figure 1(d). Error bars represent 1 standard deviation throughout the paper. For figure 1(d), however, the error bars are too small to see. Unlike Ba and Sr doping, the lattice constants a and c do not monotonically change with Ca and Mn doping, which can also be shown in the figure 1(b). In figure 1(b), (0 1 2), (1 1 0) and (1 1 1) peaks do not move in the same direction with increasing doping level. This can be attributed to the much closer atomic radius of La $^{3+}$ (0.106 nm) and Ca $^{2+}$ (0.099 nm).

In figure 2(a), we show dc magnetization of (La $_{1-x}$ Ca $_x$)(Zn $_{1-x}$ Mn $_x$)AsO ($x = 0.05, 0.10, 0.20$) measured with $B_{ext} = 0.1$ T under both zero-field-cooled (ZFC) and field-cooled (FC) conditions. We observe a significant increase in magnetization at $T_C \sim 25$ K for $x = 0.05$, and a bifurcation of ZFC and FC curves at ~ 10 K. The bifurcation between ZFC

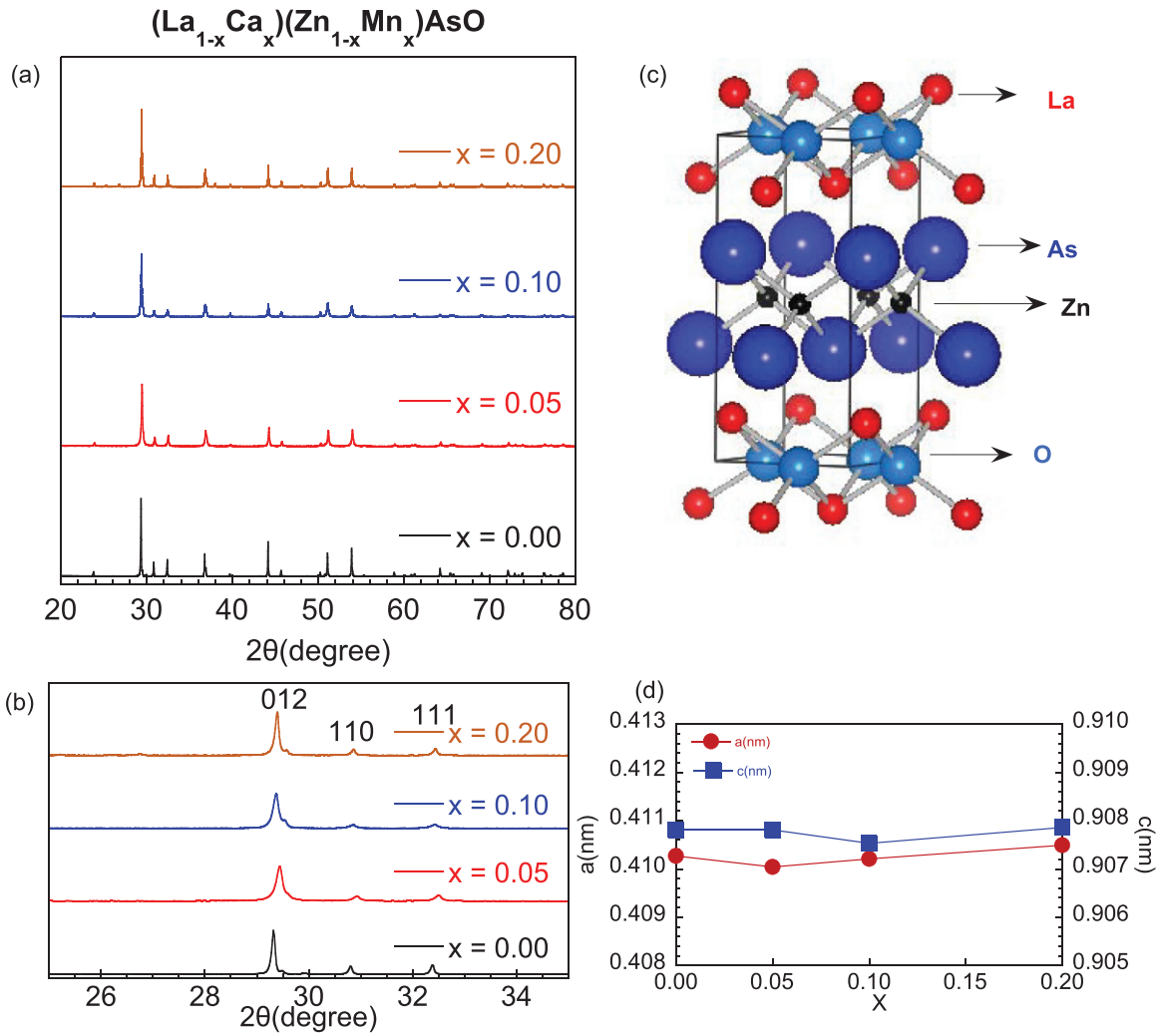


Figure 1. (a) Powder x-ray diffraction pattern of $(La_{1-x}Ca_x)(Zn_{1-x}Mn_x)AsO$ ($x = 0.00, 0.05, 0.10, 0.20$). (b) Magnified view of (0 1 2), (1 1 0), and (1 1 1) peak for $(La_{1-x}Ca_x)(Zn_{1-x}Mn_x)AsO$. (c) Crystal structure of $LaZnAsO$. (d) Lattice parameters for a axis (red solid circles) and c axis (blue solid squares) of $(La_{1-x}Ca_x)(Zn_{1-x}Mn_x)AsO$ ($x = 0.00, 0.05, 0.10, 0.20$).

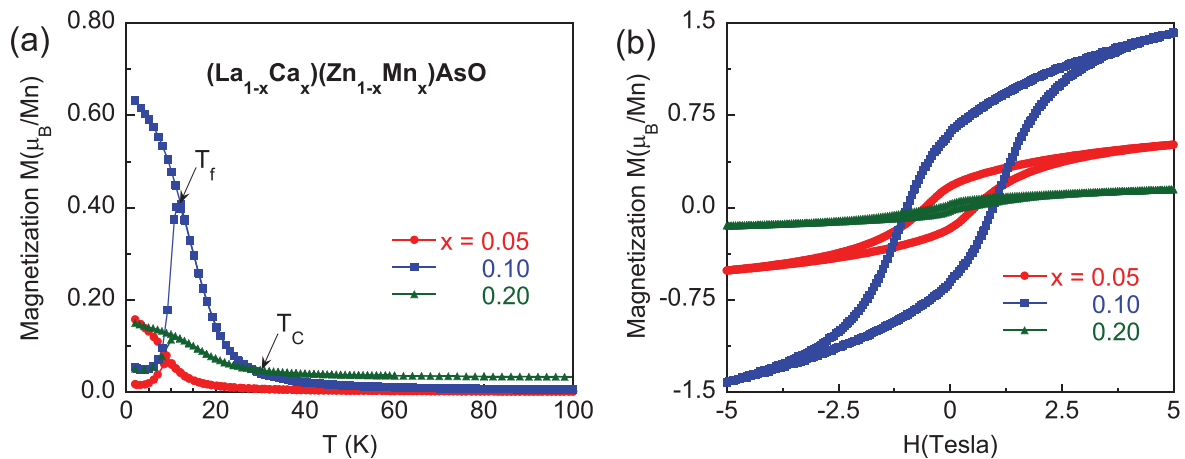


Figure 2. (a) dc magnetization measurements under ZFC and FC for $(La_{1-x}Ca_x)(Zn_{1-x}Mn_x)AsO$ ($x = 0.05, 0.10, 0.20$) at $B_{ext} = 0.1$ T; T_C and T_f are marked by arrows. (b) The isothermal magnetization measurements for $(La_{1-x}Ca_x)(Zn_{1-x}Mn_x)AsO$ ($x = 0.05, 0.10, 0.20$) at 5 K.

and FC curves maybe a result of formation and motion of magnetic domains. The temperature of the bifurcation is defined as T_f , the onset temperature of static spin freezing. When the concentration of Ca and Mn is increased up to $x = 0.10$ and 0.20 ,

the ferromagnetic Curie temperature T_C increases to 30 K, and T_f increases to ~ 12 K. T_C and T_f of $x = 0.10$ are marked by arrows in figure 2(a). The saturation moment at 2 K for $x = 0.05$ is $0.158 \mu_B Mn^{-1}$, and increases to $0.639 \mu_B Mn^{-1}$

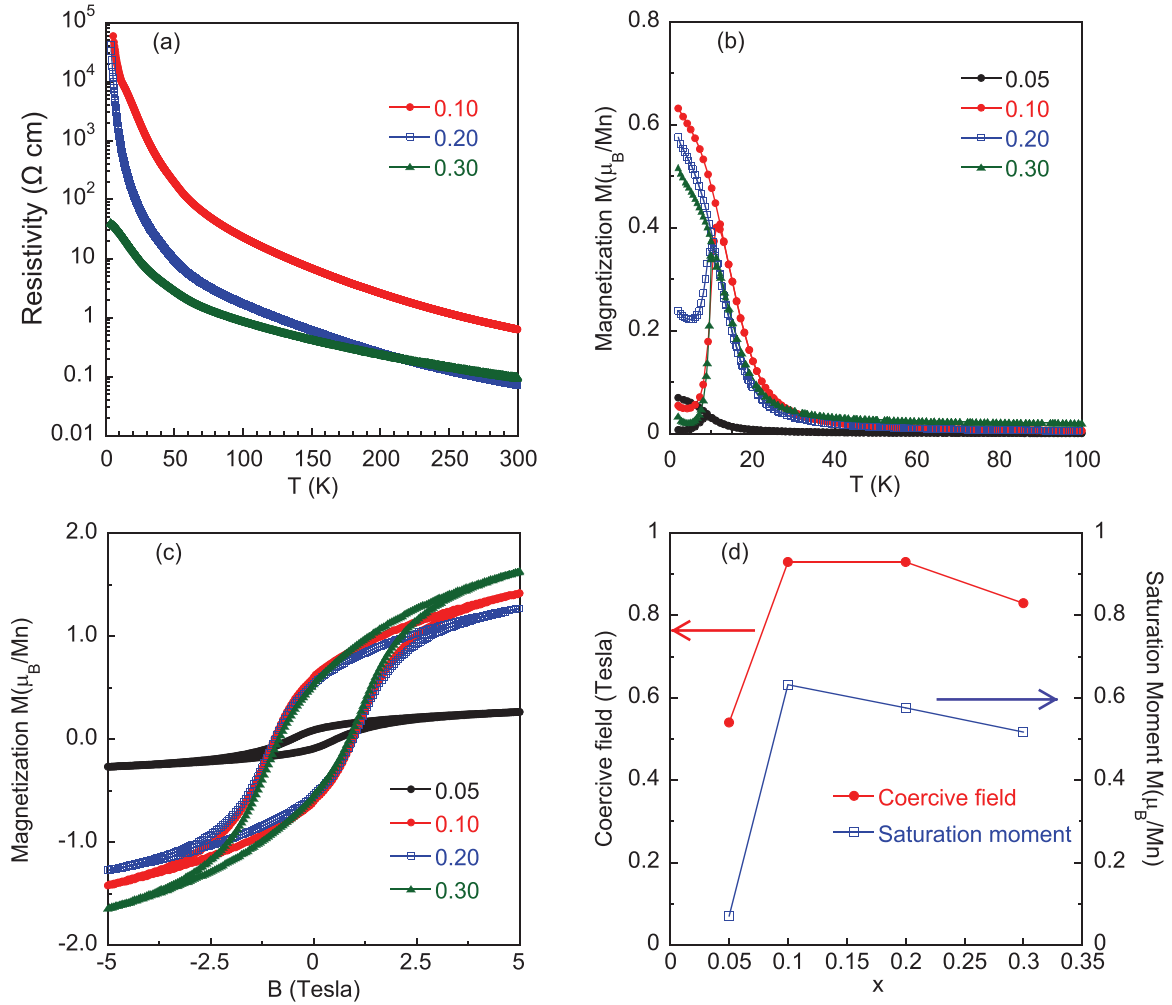


Figure 3. (a) Temperature-dependent electrical resistivity for $(\text{La}_{1-x}\text{Ca}_x)(\text{Zn}_{0.90}\text{Mn}_{0.10})\text{AsO}$ ($x = 0.10, 0.20, 0.30$). (b) dc magnetization measurements under ZFC and FC for $(\text{La}_{1-x}\text{Ca}_x)(\text{Zn}_{0.90}\text{Mn}_{0.10})\text{AsO}$ ($x = 0.05, 0.10, 0.20, 0.30$) at $B_{\text{ext}} = 1000$ Oe. (c) Isothermal magnetization measurements for $(\text{La}_{1-x}\text{Ca}_x)(\text{Zn}_{0.90}\text{Mn}_{0.10})\text{AsO}$ ($x = 0.05, 0.10, 0.20, 0.30$) at 5 K. (d) Ca concentration dependence of coercive field and saturation moment.

for $x = 0.10$, and then decreases to $0.151 \mu_B \text{ Mn}^{-1}$ with the higher doping level $x = 0.20$.

The isothermal magnetization for $(\text{La}_{1-x}\text{Ca}_x)(\text{Zn}_{1-x}\text{Mn}_x)\text{AsO}$ ($x = 0.05, 0.10, 0.20$) at 5 K is shown in figure 2(b). The high field moment at 5 K and $B_{\text{ext}} = 5$ T changes with doping level in the same way as that at 2 K and $B_{\text{ext}} = 0.1$ T. $M(5 \text{ T}) \sim 0.5 \mu_B \text{ Mn}^{-1}$ for $x = 0.05$, and increases to $M(5 \text{ T}) \sim 1.4 \mu_B \text{ Mn}^{-1}$ for $x = 0.10$, and then decreases to $M(5 \text{ T}) \sim 0.15 \mu_B \text{ Mn}^{-1}$ for $x = 0.20$. It is strange that the value of the moment for $x = 0.20$ is robust at different external fields. A parallelogram-shaped hysteresis loop shows a coercive field of 0.56 T for $x = 0.05$. The coercive field increases to 0.97 T for $x = 0.10$ and then decreases with further doping. For $x = 0.20$, the coercive field is 0.27 T. The change of coercive field with doping level is likely the result of competition between ferromagnetic coupling via the RKKY interaction [12] and the NN antiferromagnetic coupling via the direct exchange interaction. The RKKY exchange interaction can be written as $J \sim \cos(2k_F r)/r^3$, where r is the distance between two localized moments and k_F is the radius of the Fermi surface. We codope more Ca and Mn into $(\text{La,Ca})(\text{Zn,Mn})$

AsO, and introduce more hole carriers and localized spins, which modifies the Fermi surface, density of states, and ferromagnetic coupling. On the other hand, the higher doping level enhances the probability of finding two Mn atoms at NN Zn sites, and consequently the antiferromagnetic coupling. There must be a doping level which is optimal for ferromagnetic ordering. In the present work, the optimal concentration is $x \sim 0.10$. The coercive fields of $(\text{La,Ca})(\text{Zn,Mn})\text{AsO}$ are larger than that of $(\text{Ga}_{0.965}\text{Mn}_{0.035})\text{AsO}$ (~ 0.005 T) [2] and $\text{Li}_{1.1}(\text{Zn,Mn})\text{PnO}$ ($\text{Pn} = \text{As, P}$) (~ 0.01 T) [17, 18].

As stated in our earlier work [19], the detailed discrimination between ferromagnetic or spin-glass states requires the magnetization data as well as neutron scattering results. Since we cannot observe the magnetic scattering peaks due to the low average moment size, $\sim 0.06 \mu_B \text{ Mn}^{-1}(\text{Zn})$ in $(\text{La}_{0.90}\text{Ca}_{0.10})(\text{Zn}_{0.90}\text{Mn}_{0.10})\text{AsO}$ (which is smaller than the limit of neutron resolution $\sim 0.1 \mu_B$), there is no definite evidence at this moment to distinguish between ferromagnetic and spin-glass states for the present system. However, the magnitudes of ferromagnets' remnant magnetic moments in the ground state at low temperatures,

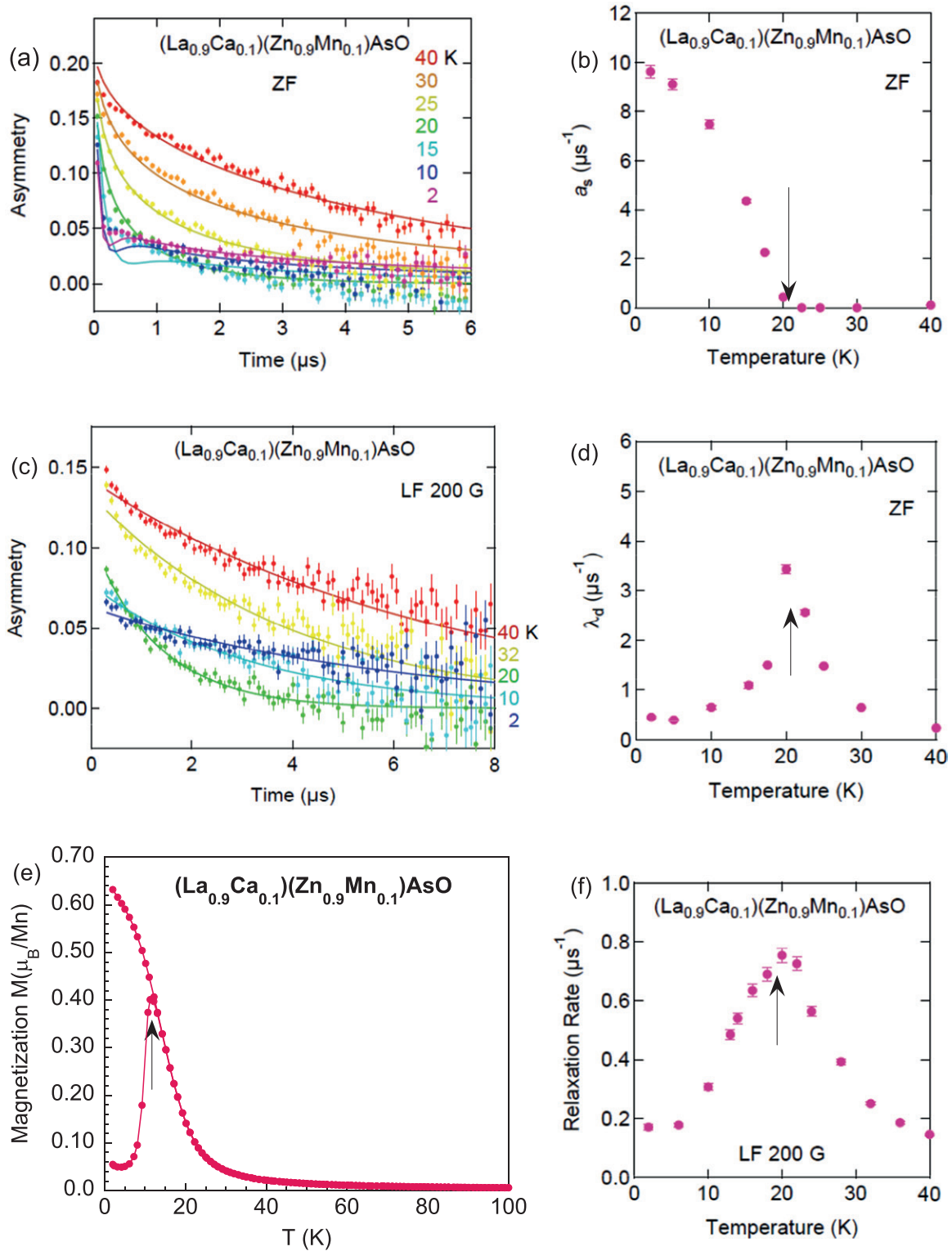


Figure 4. (a) Zero-field μ SR time spectra of $(\text{La}_{0.9}\text{Ca}_{0.1})(\text{Zn}_{0.9}\text{Mn}_{0.1})\text{AsO}$. Fits using the dynamic-static relaxation function [35] are shown as solid lines. (b) The static local field amplitude parameter a_s . (c) The time spectra of LF μ SR with a longitudinal field of 200 G for $(\text{La}_{0.9}\text{Ca}_{0.1})(\text{Zn}_{0.9}\text{Mn}_{0.1})\text{AsO}$. (d) The dynamic relaxation rate parameter λ_d . (e) dc magnetization measurements under ZFC and FC for $(\text{La}_{0.9}\text{Ca}_{0.1})(\text{Zn}_{0.9}\text{Mn}_{0.1})\text{AsO}$. (f) Muon spin relaxation rate $1/T_1$ due to dynamic spin fluctuations. The arrows in (b), (d), and (f) indicate the onset temperature of static spin freezing.

obtained in zero field after training in high external magnetic fields, is clearly different from that of spin glasses. The value of remnant magnetization for many ferromagnets is usually in the order of $1 \mu_B$ per magnetic atom, but it is only $\sim 0.01 \mu_B$ per

magnetic atom for typical dilute alloy spin glasses [32–34]. In the current system, the maximum magnetization is about $0.75 \mu_B$ per Mn, as shown in figures 2(b) and 3(c). Therefore, we tentatively assign the present system as ferromagnet.

As the next step, since the spins and carriers can be controlled separately by the doping levels of Mn and Ca, we would like to investigate the influence of the Ca concentration on the magnetism with a fixed Mn concentration. We keep the Mn concentration fixed at 10%, and change the concentration of Ca in $(\text{La,Ca})(\text{Zn,Mn})\text{AsO}$ from 5% to 30%.

In figure 3(a), we show the results of electrical resistance measured for $(\text{La}_{1-x}\text{Ca}_x)(\text{Zn}_{0.90}\text{Mn}_{0.10})\text{AsO}$ with $x = 0.10, 0.20, 0.30$. The resistivity of these specimens displays a typical semiconducting behavior and no semiconductor-metal transition occurs even with the Ca doping level up to 30%. It seems that spins induced by doped Mn atoms scatter and localize the hole carriers and hinder the transformation from semiconductor to metal. On the other hand, the resistivity decreases with more carriers introduced by Ca doping at the fixed Mn concentration 10%. The resistivity is on the order of $10^4 \Omega \text{ cm}$ for $x = 0.10$, and decreases by two orders of magnitude to $10^2 \Omega \text{ cm}$ for $x = 0.30$.

In figure 3(b), we show ZFC and FC dc magnetization of $(\text{La}_{1-x}\text{Ca}_x)(\text{Zn}_{0.90}\text{Mn}_{0.10})\text{AsO}$ ($x = 0.05, 0.10, 0.20, 0.30$) with an applied external magnetic field $B_{\text{ext}} = 0.1 \text{ T}$. For $x = 0.05$, the ferromagnetic Curie temperature T_C is $\sim 24 \text{ K}$, and the static spin freezing temperature T_f is $\sim 9 \text{ K}$. As the doping level of Ca increases to $x = 0.10$, and finally reaches $x = 0.30$, T_C increases to 30 K, and T_f increases to 12 K. The saturation moment at 2 K for $x = 0.05$ is $0.068 \mu_B \text{ Mn}^{-1}$ and increases to $0.639 \mu_B \text{ Mn}^{-1}$ for $x = 0.10$, nearly an order of magnitude larger than that of $x = 0.05$. The saturation moment starts to decrease with further increase of the Ca doping level to 0.20 ($0.566 \mu_B \text{ Mn}^{-1}$) and 0.30 ($0.503 \mu_B \text{ Mn}^{-1}$). This demonstrates that too many carriers are detrimental to ferromagnetism, which agrees with the result in $(\text{La,Sr})(\text{Zn,Mn})\text{AsO}$. The isothermal magnetization for $(\text{La}_{1-x}\text{Ca}_x)(\text{Zn}_{0.90}\text{Mn}_{0.10})\text{AsO}$ ($x = 0.05, 0.10, 0.20, 0.30$) at 5 K is shown in figure 3(c). The coercive field is 0.53 T for $x = 0.05$, and increases to 0.97 T for $x = 0.10$, then decreases with further doping. For $x = 0.20$ and 0.30, the coercive field is 0.95 T and 0.84 T, respectively. The Ca concentration dependence of both the coercive field and saturation moment of $(\text{La}_{1-x}\text{Ca}_x)(\text{Zn}_{0.90}\text{Mn}_{0.10})\text{AsO}$ are plotted in figure 3(d). They all increase with the doping level of Ca increasing up to $x = 0.10$ from $x = 0.05$, and then decrease monotonically when x is between 0.10 and 0.30. The Ca concentration dependence of the coercive field and saturation moment is likely due to the hole-carrier-mediated RKKY interaction for spins [12]. Since the concentration of hole carriers induced by Ca modifies the shape of Fermi surface and affects the ferromagnetic ordering, it requires a proper balance of carriers and spins to make the RKKY interaction optimal for ferromagnetism. Considering from figure 3(d) that the maximum of the coercive field and saturation moment with the Mn concentration fixed at 10% is the sample with Ca doping of 10%, we may come to the conclusion that the one-to-one ratio of Ca and Mn doping is the best for ferromagnetism in $(\text{La,Ca})(\text{Zn,Mn})\text{AsO}$.

A robust value of T_C and a slight reduction of the saturation moment and the coercive field are observed in $(\text{La}_{1-x}\text{Ca}_x)(\text{Zn}_{0.90}\text{Mn}_{0.10})\text{AsO}$ as the Ca doping level is increased from 10% to 30%. This is different from $(\text{La}_{1-x}\text{Sr}_x)(\text{Zn}_{0.90}\text{Mn}_{0.10})\text{AsO}$, where T_C , saturation moment and coercive field are all

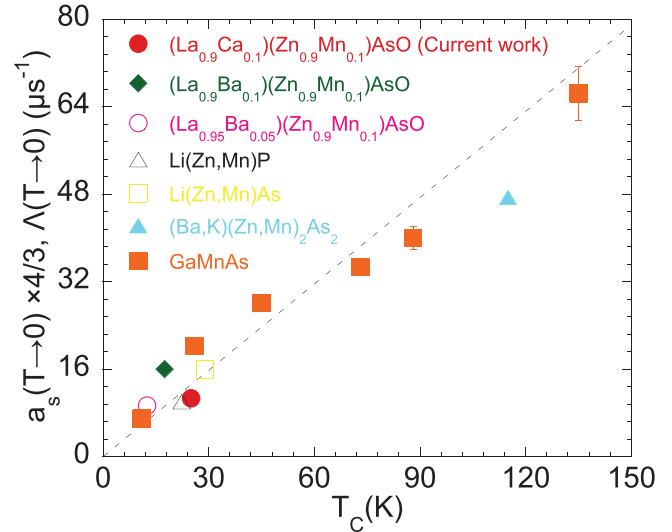


Figure 5. The ferromagnetic Curie temperature T_C dependence on the static internal field parameter a_s measured in $\text{Li}(\text{Zn,Mn})\text{As}$ [17], $\text{Li}(\text{Zn,Mn})\text{P}$ [29], $(\text{La,Ba})(\text{Zn,Mn})\text{AsO}$ [19], $(\text{La,Ca})(\text{Zn,Mn})\text{AsO}$, $(\text{Ba,K})(\text{Zn,Mn})\text{AsO}$ [23] and $(\text{Ga,Mn})\text{As}$ [30].

heavily reduced when the doping level of Sr increases to 30%. The different behaviors of $(\text{La}_{1-x}\text{Ca}_x)(\text{Zn}_{0.90}\text{Mn}_{0.10})\text{AsO}$ and $(\text{La}_{1-x}\text{Sr}_x)(\text{Zn}_{0.90}\text{Mn}_{0.10})\text{AsO}$ with same doping level of carriers are probably due to the different atomic radius between Ca^{2+} (0.099 nm) and Sr^{2+} (0.113 nm). The radius of Ca^{2+} is much smaller than that of Sr^{2+} , which consequently influences the distances, and therefore the interactions between spins and carriers. In other words, a larger effect of scattering and localization takes place in $(\text{La,Ca})(\text{Zn,Mn})\text{AsO}$ with a smaller lattice constant. This explanation is also consistent with the results of electrical resistance measurements. The value of resistivity at low temperature for $(\text{La}_{0.90}\text{Ca}_{0.10})(\text{Zn}_{0.90}\text{Mn}_{0.10})\text{AsO}$ in figure 3(a) is about one order of magnitude larger than that for $(\text{La}_{0.90}\text{Sr}_{0.10})(\text{Zn}_{0.90}\text{Mn}_{0.10})\text{AsO}$ [20], which suggesting the spins scattering and localizing the carriers in $(\text{La}_{0.90}\text{Ca}_{0.10})(\text{Zn}_{0.90}\text{Mn}_{0.10})\text{AsO}$ more heavily than in $(\text{La}_{0.90}\text{Sr}_{0.10})(\text{Zn}_{0.90}\text{Mn}_{0.10})\text{AsO}$. The different values of the temperature-dependent resistivity also indicate that the effective carrier concentration of $(\text{La}_{1-x}\text{Ca}_x)(\text{Zn}_{0.90}\text{Mn}_{0.10})\text{AsO}$ is lower than that of $(\text{La}_{1-x}\text{Sr}_x)(\text{Zn}_{0.90}\text{Mn}_{0.10})\text{AsO}$. Such phenomena demonstrate that the lower but more robust T_C in $(\text{La}_{1-x}\text{Ca}_x)(\text{Zn}_{0.90}\text{Mn}_{0.10})\text{AsO}$ may be due to the lower effective carrier concentration.

In order to investigate the spin dynamics, we performed μSR measurements on $(\text{La}_{0.90}\text{Ca}_{0.10})(\text{Zn}_{0.90}\text{Mn}_{0.10})\text{AsO}$ specimen. The time spectra of ZF- μSR for $(\text{La}_{0.90}\text{Ca}_{0.10})(\text{Zn}_{0.90}\text{Mn}_{0.10})\text{AsO}$ from 2 K to 40 K are shown in figure 4(a). Below 30 K, the muon spin relaxation shows an obvious increase in relaxation rate. The behavior of this ZF- μSR time spectra is similar to spin glass systems, like AuFe and CuMn, where AuFe and CuMn exhibit characteristic signatures of dynamic slowing down followed by static magnetic order [35]. Nevertheless, for the '1 1 1' ($\text{Li}(\text{Zn,Mn})\text{Pn}$ ($\text{Pn} = \text{As, P}$)) system [17, 29], the ZF time spectra can be analyzed by the two component function. One component represents the magnetically ordered volume with the internal static magnetic field distribution modeled as a Lorentzian distribution. The other component

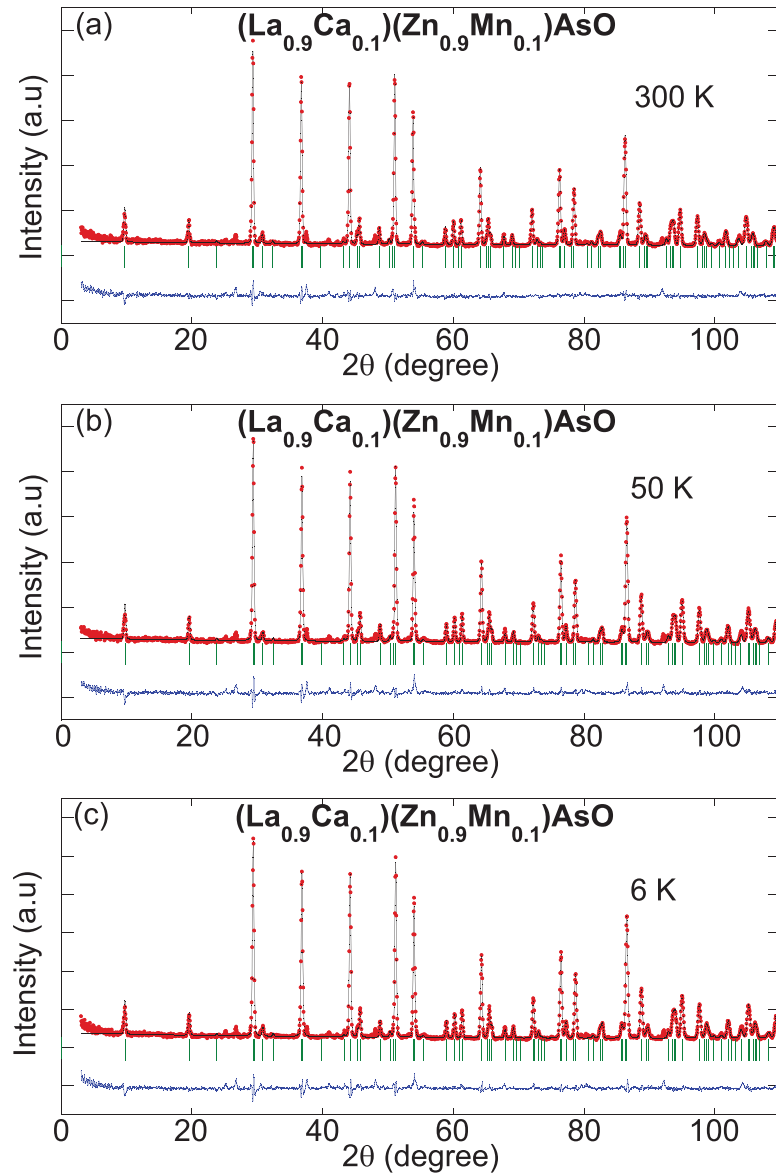


Figure 6. Neutron diffraction pattern for a powder specimen of $(\text{La}_{0.9}\text{Ca}_{0.1})(\text{Zn}_{0.9}\text{Mn}_{0.1})\text{AsO}$ at 300 K (a), 50 K (b) and 6 K (c) at NIST

represents the remaining paramagnetic volume expressed as an exponentially decaying dynamic relaxation function. The refined static random field amplitude a_s and dynamic relaxation rate λ_d extracted from the fitting of ZF time spectra are plotted in figures 4(b) and (d). When fitting the data of ZF time spectra, we used a_s and λ_d as the only free parameters. The refined static random field amplitudes a_s is the width of static field distribution, which is proportional to the spin S of impurity moments at $T = 0$ and the static polarization at finite temperature [35]. The dynamic relaxation λ_d equals to $4a_d^2/\nu$, where a_d is the dynamic fluctuating field and ν is the fluctuation rate of the random field [35].

The time spectra of LF- μ SR for $(\text{La}_{0.90}\text{Ca}_{0.10})(\text{Zn}_{0.90}\text{Mn}_{0.10})\text{AsO}$ at LF = 200 G are plotted in figure 4(c). In figure 4(f), we show the LF relaxation rate $1/T_1$. We observe a clear peak at ~ 20 K. This value is the same as the temperature where a_s suddenly increases (figure 4(b)) and λ_d reaches a maximum (figure 4(d)). For comparison, we reproduce the ZFC and FC dc magnetization of $(\text{La}_{0.90}\text{Ca}_{0.10})(\text{Zn}_{0.90}\text{Mn}_{0.10})\text{AsO}$

measured under $B_{\text{ext}} = 0.1$ T in figure 4(e). The departure temperature of ZFC and FC magnetization occurs at 15–20 K. The consistency of ~ 20 K from figures 4(b), (d)–(f) suggests that 20 K is the onset temperature of the static spin freezing.

We plot $(4/3) \times a_s$ at low temperature versus T_C for $(\text{La}_{0.90}\text{Ca}_{0.10})(\text{Zn}_{0.90}\text{Mn}_{0.10})\text{AsO}$ in figure 5. A factor of $4/3$ is multiplied to a_s to adjust the difference between a_s and the simple exponential decay rate Λ (For a detail explanation, please refer to the supplement materials of [17]). a_s falls onto the linear relation observed for $(\text{Ga},\text{Mn})\text{As}$ [30], $\text{Li}(\text{Zn},\text{Mn})\text{As}$ [17], $\text{Li}(\text{Zn},\text{Mn})\text{P}$ [29], $(\text{Ba},\text{K})(\text{Zn},\text{Mn})_2\text{As}_2$ [23] and $(\text{La},\text{Ba})(\text{Zn},\text{Mn})\text{AsO}$ [19]. The local field amplitude parameter a_s is proportional to the individual ordered moment size multiplied by the moment concentration, and the ferromagnetic Curie temperature T_C is a measurement of the effective average ferromagnetic interaction. Therefore the linear relation between a_s and T_C , suggests that the ferromagnetic exchange interaction in these DMS systems share a common mechanism. Never the less, as stated in reference 19 and 20, $\text{La}(\text{Zn}_{0.90}\text{Mn}_{0.10})\text{AsO}$

remains paramagnetic down to 2 K without carriers. This indicates that the ferromagnetic ordering develops only when the spins are mediated by carriers, which is similar to the case of the (Ga,Mn)As system where Zener's model [12] is proposed as one candidate to explain the ferromagnetism. The study of current DMS system may help to understand the origin of ferromagnetism in (Ga,Mn)As and other III–V DMSs.

We also conducted neutron diffraction measurements on a powder specimen of $(\text{La}_{0.90}\text{Ca}_{0.10})(\text{Zn}_{0.90}\text{Mn}_{0.10})\text{AsO}$, from 6 K to 300 K at NCNR to look for signals of long range magnetic ordering. The results are shown in figure 6. Firstly, we do not observe any impurities, consistent with the x-ray diffraction pattern shown in figure 1. This again indicates the successful Mn substitution for Zn. Furthermore, we do not observe any structural phase transition over the measured temperature range. By comparing the neutron diffraction data collected at 6 K (which is below $T_f \sim 20$ K and $T_C \sim 30$ K) with that measured at 50 K, we can not distinguish any magnetic Bragg peaks from the structural ones. We note that the Mn saturated moments is $0.639 \mu_B \text{Mn}^{-1}$ for this concentration, and the average moment size is only $\sim 0.06 \mu_B \text{Mn}^{-1}(\text{Zn})$. This value is smaller than the limit of $\sim 0.1 \mu_B$ for the current neutron diffraction configuration.

4. Summary and conclusion

To summarize, we successfully synthesized a new DMS system $(\text{La}_{1-x}\text{Ca}_x)(\text{Zn}_{1-y}\text{Mn}_y)\text{AsO}$, with the maximum $T_C \sim 30$ K. We find for the fixed Mn doping level of $y = 0.1$, both the coercive field and the saturation moment increase when the doping level of Ca increases from $x = 5\%$ to $x = 10\%$, and then decrease monotonically with further Ca doping up to $x = 30\%$. Our results indicate that equal concentrations of carriers and spins is best to optimize the ferromagnetic ordering, and too few or too many carriers are detrimental to the ferromagnetic ordering. The different magnetic behaviors between $(\text{La}_{1-x}\text{Ca}_x)(\text{Zn}_{0.9}\text{Mn}_{0.1})\text{AsO}$ and $(\text{La}_{1-x}\text{Sr}_x)(\text{Zn}_{0.9}\text{Mn}_{0.1})\text{AsO}$ indicate that a lower effective carrier concentration may leads to a lower but more robust T_C . μSR experiments demonstrated that $(\text{La,Ca})(\text{Zn,Mn})\text{AsO}$ has a common mechanism for the ferromagnetic exchange interaction with (Ga,Mn)As, which is helpful to understand the origin of ferromagnetism in III–V DMSs. Our neutron scattering experiments do not show a structural transition between 300 K and 6 K for $(\text{La}_{0.90}\text{Ca}_{0.10})(\text{Zn}_{0.90}\text{Mn}_{0.10})\text{AsO}$. In addition, as mentioned in the previous papers, $(\text{La,Ca})(\text{Zn,Mn})\text{AsO}$ is isostructural to the Fe-based superconductor LaFeAsO [14] and the antiferromagnetic LaMnAsO [31], offering the opportunity to develop junction devices based on these three systems.

Acknowledgments

The work at Zhejiang was supported by National Basic Research Program of China (No. 2014CB921203), NSF of China (No. 11274268 and 11574265), Zhejiang Provincial Natural Science Foundation of China (No. LR15A040001); at Columbia by the U.S. NSF PIRE (Partnership for International Research and Education, Grant No. OISE-0968226) and Grant No. DMR-1105961 and CMREF grant no. NSF

DMR-1436095; the JAEA Reimei Project at IOP, Columbia, PSI. F L Ning acknowledges helpful discussions with C Q Jin. The identification of any commercial product or trade name does not imply endorsement or recommendation by the National Institute of Standards and Technology.

References

- [1] Munekata H, Ohno H, von Molnar S, Segmuller A, Chang L L and Esaki L 1849 *Phys. Rev. Lett.* **63** 1849
- [2] Ohno H, Shen A, Matsukura F, Oiwa A, Endo A, Katsumoto S and Iye Y 1996 *Appl. Phys. Lett.* **69** 363
- [3] Zutic I, Fabian J and Das Sarma S 2004 *Rev. Mod. Phys.* **76** 323
- [4] Jungwirth T, Sinova J, Masek J, Kucera J and MacDonald A H 2006 *Rev. Mod. Phys.* **78** 809
- [5] Samarth N 2010 *Nat. Mater.* **9** 955
- [6] Chambers S 2010 *Nat. Mater.* **9** 956
- [7] Dietl T 2010 *Nat. Mater.* **9** 965
- [8] Dietl T and Ohno H 2014 *Rev. Mod. Phys.* **86** 187
- [9] Wang M, Campion R P, Rushforth A W, Edmonds K W, Foxon C T and Gallagher B L 2008 *Appl. Phys. Lett.* **93** 132103
- [10] Chen L, Yan S, Xu P F, Wang W Z, Deng J J, Qian X, Ji Y and Zhao J H 2009 *Appl. Phys. Lett.* **95** 182505
- [11] Chen L, Yang X, Yang F H, Misuraca J, Xiong P, Molnar S V and Zhao J H 2011 *Nano. Lett.* **11** 2584
- [12] Dietl T, Ohno H, Matsukura F, Cibert J and Ferrand D 2000 *Science* **287** 1019
- [13] Wang X C, Liu Q Q, Lv Y X, Gao W B, Yang L X, Yu R C, Li F Y and Jin C Q 2008 *Solid State Commun.* **148** 538
- [14] Kamihara Y, Watanabe T, Hirano M and Hosono H 2008 *J. Am. Chem. Soc.* **130** 3296
- [15] Rotter M, Tegel M and Johrendt D 2008 *Phys. Rev. Lett.* **101** 107006
- [16] Shirage P M, Kihou K, Lee C H, Kito H, Eisaki H and Iyo A 2011 *J. Am. Chem. Soc.* **133** 9630
- [17] Deng Z et al 2011 *Nat. Commun.* **2** 422
- [18] Deng Z et al 2013 *Phys. Rev. B* **88** 081203
- [19] Ding C et al 2013 *Phys. Rev. B* **88** 041102
- [20] Ding C, Gong X, Man H Y, Zhi G X, Guo S L, Zhao Y, Wang H D, Chen B and Ning F L 2014 *Europhys. Lett.* **107** 17004
- [21] Han W, Zhao K, Wang X C, Liu Q Q, Ning F L, Deng Z, Liu Y, Ding C and Jin C Q 2013 *Sci. China Phys. Mech. Astron.* **56** 2026
- [22] Yang X J, Li Y K, Shen C Y, Si B Q, Sun Y L, Tao Q, Cao C, Xu Z A and Zhang F C 2013 *Appl. Phys. Lett.* **103** 022410
- [23] Zhao K et al 2013 *Nat. Commun.* **4** 1442
- [24] Yang X J et al 2013 *J. Appl. Phys.* **114** 223905
- [25] Man H Y, Qin C, Ding C, Wang Q, Gong X, Guo S L, Wang H D, Chen B and Ning F L 2014 *Europhys. Lett.* **105** 67004
- [26] Wang Q, Man H Y, Ding C, Gong X, Guo S L, Wang H D, Chen B and Ning F L 2014 *J. Appl. Phys.* **115** 083917
- [27] Lu J C et al 2013 *Europhys. Lett.* **103** 67011
- [28] Ding C, Qin C, Man H Y, Imai T and Ning F L 2013 *Phys. Rev. B* **88** 041108
- [29] Ning F L et al 2014 *Phys. Rev. B* **90** 085123
- [30] Dunsiger S R et al 2010 *Nat. Mater.* **9** 299
- [31] Emery N, Wildman E J, Skakle J M S, Mclaughlin A C, Smith R I and Fitch A N 2011 *Phys. Rev.* **83** 144429
- [32] Tholence J L and Tournier R 1974 *J. Phys.* **35** C4–229
- [33] Prejean J J, Joliclerc M J and Monod P 1980 *J. Phys.* **41** 427
- [34] Monod P, Prejean J J and Tissier B 1979 *J. Appl. Phys.* **50** 7324
- [35] Uemura Y J, Yamazaki T, Harshman D R, Senba M and Ansaldo E J 1985 *Phys. Rev. B* **31** 546